Mesoscale fractures control the scale dependences of seismic velocity and fluid flow in subduction zones

Yuya Akamatsu[1*], Hanaya Okuda[2], Manami Kitamura[3], Michiyo Sawai[4]

1. Research Institute for Marine Geodynamics, Japan Agency for Marine-Earth Science and Technology (JAMSTEC), Japan
2. Kochi Institute for Core Sample Research, Japan Agency for Marine-Earth Science and Technology (JAMSTEC), Japan
3. Research Institute of Geo-Resources and Environment, Geological Survey of Japan, National Institute of Advanced Industrial Science and Technology, Japan
4. Department of Earth Sciences, Chiba University, Japan

* Corresponding author: Yuya Akamatsu (akamatsuy@jamstec.go.jp)

This is a non-peer reviewed preprint submitted to EPSL.

Abstract

Natural geological systems contain porosity structures of various scales that play different roles in geophysical properties, fluid flow, and geodynamics. To understand seismic activity associated with high pore-fluid pressure and fluid migration in subduction zones, it is necessary to explore the scale dependence of geophysical properties such as seismic velocity and permeability. Here, we compare laboratory-measured ultrasonic velocity (1 MHz) measured on core samples from the Susaki area in the Shimanto accretionary complex, SW Japan, with sonic velocity (15 kHz) measured by borehole logging experiments. Results show that P-wave velocity decreases from the laboratory (~6 km/s) to the borehole scales (~5 km/s). This scale-variant effect can be explained by a differential effective medium model whereby mesoscale porosity that is undetectable at the ultrasonic wavelength is introduced into the matrix phase with microscale porosity. Assuming typical apertures for micro- and mesoscale fractures, we estimate that the effective permeability can increase to 10^{-12}–10^{-11} m^2 with increasing in the mesoscale porosity and decreasing P-wave velocity down to 4–5 km/s. These results indicate that seismic velocity anomalies and related seismic activity are associated with the presence of mesoscale fractures in subduction zones.

Highlights

- Measured P-wave velocity decreases from laboratory to borehole scales
- Presence of mesoscale fractures is indicated by upscaled effective medium modeling
- Mesoscale fractures can facilitate rapid fluid drainage in subduction zones

Keywords

seismic velocity; upscaling; permeability; Nankai Trough

1 Introduction

Seismic activity in subduction zones has been related to high-pore fluid pressure and the properties of the fluid drainage system on the basis that fluids play a dominant role in controlling the frictional and rheological properties of rock (Saffer and Tobin, 2011). As pore fluid can also influence the elastic properties of rock (Mavko et al., 2020), seismic velocity structures have been obtained by seismological surveys and borehole logging in various subduction zones to understand the causes of seismic activity (e.g., Audet and Schwartz, 2013; Eberhart-Phillips et al., 2017; Kamei et al., 2013; Saffer, 2003; Shiraishi et al., 2019). These velocity structures have revealed low-velocity anomalies and episodic changes in velocity along the plate boundaries, which are likely associated with the presence of high pore-fluid pressure and transient fluid migration (Tonegawa et al., 2022; Tsuji et al., 2014).

To link seismic velocity and the pore fluid state, laboratory measurements of elastic wave velocity using rock samples from the Nankai subduction zone, including drillcore from the seafloor and an ancient accretionary complex on land, have been conducted (Hamahashi et al., 2013; Hoffman and Tobin, 2004; Kitamura et al., 2021; Raimbourg et al., 2011). These studies have revealed the role of microscopic pores and cracks in controlling elastic wave velocity, which has been applied to interpretations of observed seismic velocity structures (Kitajima and Saffer, 2012; Tsuji et al., 2014). However, there is a large gap in the scales of observations among laboratory measurements, borehole logging, and seismic surveys, primarily because of the different probing frequencies and hence different wavelengths for measurements at each scale. Laboratory measurements are typically carried out at ultrasonic frequency (~MHz) with hand-sized samples, and the measured elastic wave velocity reflects millimeter-scale structures, such as microcracks and pores. In contrast, borehole sonic logging and seismological surveys are performed typically at frequencies of ~kHz and ~Hz, respectively, which correspond to wavelengths of meters to kilometers. Given that natural geological systems are heterogeneous and contain defects of different scales at each scale of observation, the observed sonic and seismic velocities at relatively low frequencies should be affected not only by microscopic pore structures but also by larger-scale defects, such as fractures and faults (Bailly et al., 2019; Matonti et al., 2015). As the permeability of rocks depends strongly on the dimensions of conduits, such large-scale defects can lead to more effective fluid drainage compared with microscopic pores and cracks, and may be related to the episodic occurrence of slow slip and tremor associated with rapid fluid migration along subduction plate interfaces (Ide, 2010; Muñoz-Montecinos and Behr, 2023). It is therefore crucial to explore the scale dependence of elastic wave velocity to quantitatively relate the seismic velocity structures to seismic activity in subduction zones via pore fluid behavior.

This study aims to obtain porosity structures at two scales (micro- and mesoscales) in a rock mass sourced from a deep subduction zone and estimate the contribution of pore fulid to seismic velocity at each scale. We use core samples from the Cretaceous Shimanto belt in the Susaki area, Kochi, SW Japan, which is originated from the depths of seismogenic zone in a subduction zone similar to the present-day Nankai Trough (Itaba et al., 2014). We first measured the P-wave velocity of the core samples at the MHz frequency and dense intervals to obtain spatial variations in microscopic porosity at a macroscopic scale. We then compared our data with sonic logging velocities measured at the kHz frequency in the borehole. Results show a decrease in the P-wave velocity at larger scales, suggesting the presence of mesoscale fractures. Finally, we estimated the effective permeability of the rock at each scale, and discuss the potential role of mesoscale fractures on seismic velocity and fluid flow in subduction zones.

2 Geologic setting and borehole logging data

The Susaki area is located in the Cretaceous Shimanto belt in SW Japan, which consists of an accretionary complex associated with a plate subduction similar to the modern Nankai Trough (Fig. 1). Drilling was conducted in this area by the Geological Survey of Japan (GSJ) in 2009, and continuous cores of ~600 m in total length were recovered (Itaba et al., 2014). The drillcores consist mainly of sandstones and mudstones with intercalations of tuff layers, as well as quartz and calcite veins. Visual descriptions of the core samples revealed few major faults in the core, with mélange-like deformation being observed throughout the entire core (Itaba et al., 2014). As the drilling site is located in the area which can be geologically extended from the Yokonami mélange and Awa mélange (Taira, 1988), the core is presumed to have undergone a similar subduction–exhumation history to the two mélanges. According to the previous studies that utilized fluid inclusion analysis and vitrinite reflectance geothermometry, the mélanges reached a depth equivalent to ~200 ºC (i.e., the seismogenic zone depths) during the late Cretaceous and were then exhumed (Hashimoto et al., 2012; Sakaguchi, 1999). This history indicates that the entire core section from the Susaki area underwent the same subduction–exhumation history as these mélanges.

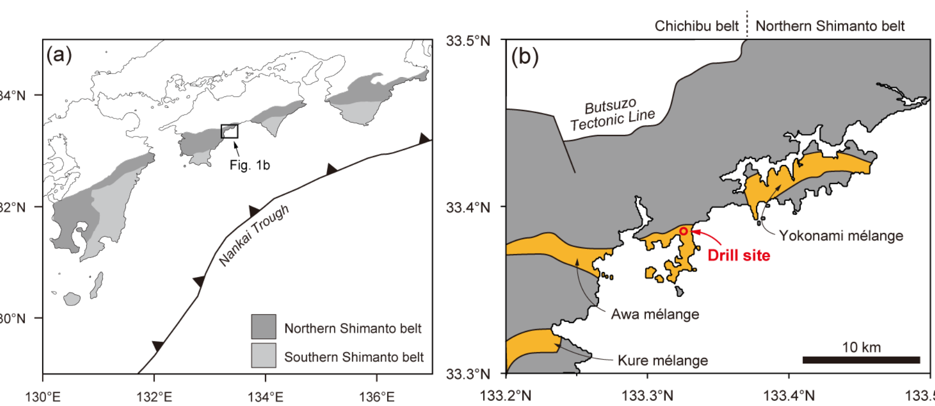

Fig. 1 (a) Geological map of SW Japan; (b) map of the area around the site of the Susaki drillhole (modified after Hashimoto et al., 2012). Colored areas are mélange zones.

Geophysical logging measurements in the studied boreholes were conducted by GSJ, and downhole physical properties were obtained, including sonic velocity, electrical resistivity, and natural gamma rays (Itaba et al., 2014). Here, we focus on the sonic velocity data for comparison with ultrasonic velocity. Sonic logging was conducted at a probe frequency of ~15 kHz, which corresponds to a wavelength of ~0.3 m. This means that the downhole profile in sonic velocity reflects variations in submeter-scale structures. P-wave velocity from sonic logging was determined by picking the onset of the waveforms at each 10 cm increment in depth. During sonic logging, the hole was saturated with groundwater, so the measured velocities should be considered as values under water-saturated conditions. Although the sonic P-wave velocity shows an overall monotonic depth trend ranging from 4 to 5.5 km/s (median of 5.0 km/s), sandstone layers tend to have slightly higher velocities than mudstone layers (Fig. 2).

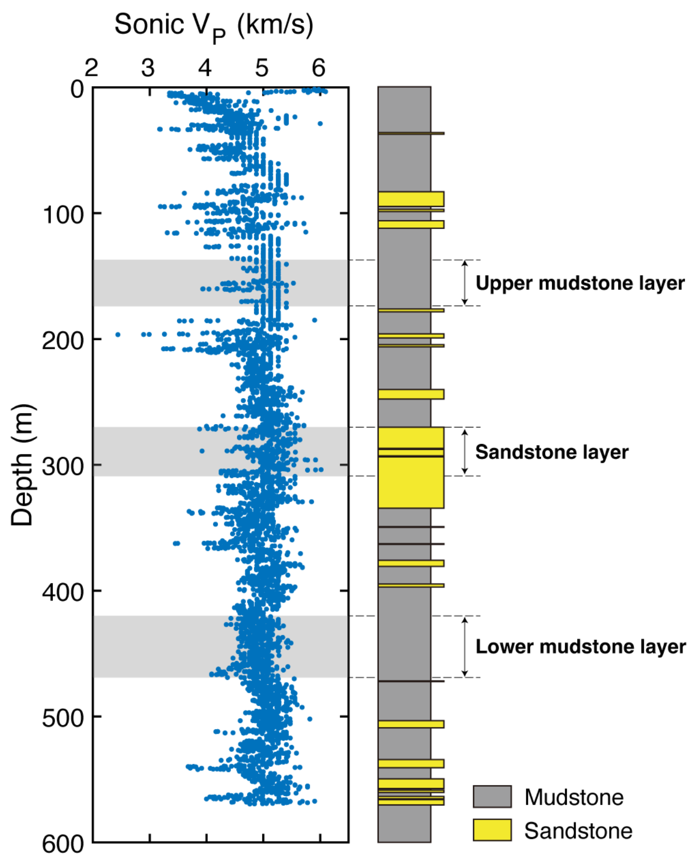

Fig. 2 Downhole profile of P-wave velocity obtained by sonic logging in the Susaki boreholes and stratigraphic column of the core samples (modified after Itaba et al., 2014). Gray shading indicates the core intervals subjected to ultrasonic velocity measurements in this study.

3 Method

3.1 Measurement of ultrasonic velocity

To evaluate the spatial distribution of microscopic porosity in the Susaki core samples, we performed dense measurements of ultrasonic P-wave velocity under dry conditions at room temperature and pressure. Measurements were performed on whole core sections from the following intervals (Fig. 2): 137–175 m (upper mudstone layer), 270–310 m (sandstone layer), and 420–470 m (lower mudstone layer). The core sections from these depths were reasonably intact and retained a cylindrical shape. P-wave velocity at the ultrasonic frequency was determined using a pulse transmission method, in which travel times of ultrasonic waves passing through the core were measured. The core sections were sandwiched by a pair of ultrasonic transducers with a resonant frequency of 1 MHz in the direction orthogonal to the core axis. An input pulse with an amplitude of 10 V was sent to the transducer by a pulse generator and was transmitted through the core, with the output signal being received by another transducer mounted on the opposite side and digitalized by an oscilloscope. The time of the first arrival of the ultrasonic wave was determined using the Akaike Information Criterion (Akamatsu et al., 2023; Sarout et al., 2009), and the P-wave velocity was then calculated by dividing the core diameter (56.5 mm for upper mudstone layer and 63.2 mm for sandstone and lower mudstone layers) by the travel time (Fig. 3). This procedure was performed at each 5 cm interval for each core section over a total length of 128 m.

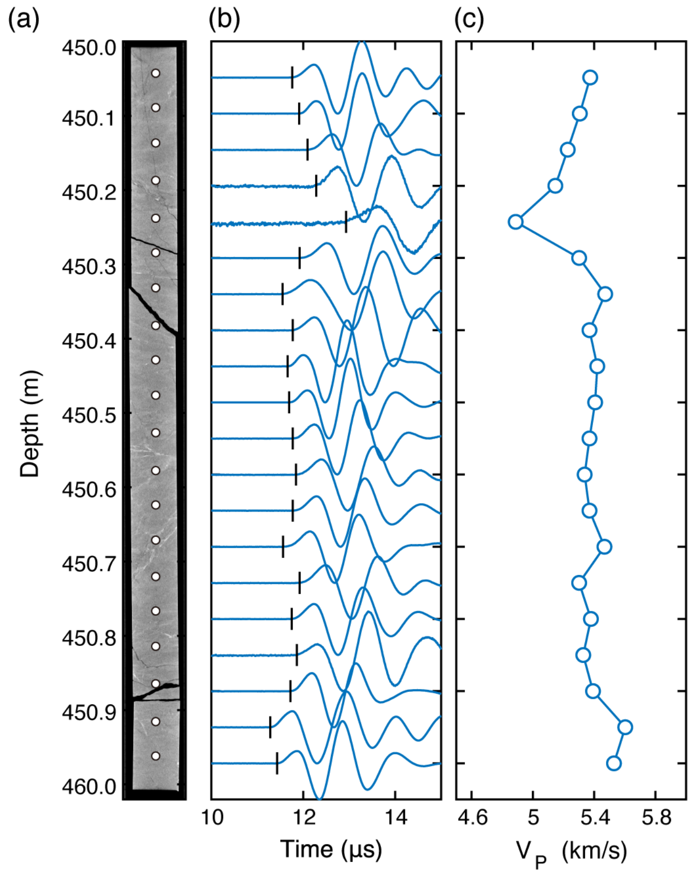

Fig. 3 Example of results of ultrasonic velocity measurements. (a) Cross-section of a core sample (depths range 445–446 m) imaged using X-ray computed tomography. (b) Waveforms recorded at points indicated by white dots in (a). Vertical black lines denote the arrival times determined by the AIC. (c) Calculated P-wave velocities.

3.2 Effective medium modeling

Although the ultrasonic velocity measurements were performed under dry conditions, the borehole logging measurements from the Susaki boreholes were carried out under groundwater-saturated conditions. It is therefore necessary to correct the ultrasonic velocity for water-saturated (wet) conditions for accurate comparison with the sonic logging velocity. Effective medium theory allows us to predict the velocity under wet conditions from that under dry conditions if porosity and pore geometry are known. Here, we employed the differential effective medium (DEM) model (Berryman et al., 2002; Mavko et al., 2020). For an isotropic medium containing randomly oriented spheroidal (penny-shaped) pores, the effective bulk modulus K^* and shear modulus G^* can be calculated as follows:

$$(1-\phi)\frac{d}{d\phi}[K^*(\phi)] = (K_i - K^*(\phi))\,P^*(\phi), \tag{1}$$

$$(1-\phi)\frac{d}{d\phi}[G^*(\phi)] = (G_i - G^*(\phi))\,Q^*(\phi), \tag{2}$$

with initial conditions $K^*(0) = K_0$ and $G^*(0) = G_0$, where K_0 and G_0 are the bulk and shear moduli of the porosity-free material, respectively; K_i and G_i are the bulk and shear moduli of the pore-filling phase, respectively; and ϕ is the porosity. P^* and Q^* are the volumetric and deviatoric strain concentration factors for a penny-shaped pores (cracks), respectively, described as follows:

$$P^* = \frac{K^* + \frac{4}{3}G_i}{K_i + \frac{4}{3}G_i + \pi\alpha\beta^*}, \tag{3}$$

$$Q^* = \frac{1}{5}\left[1 + \frac{8G^*}{4G_i + \pi\alpha(G^* + 2\beta^*)} + \frac{2K_i + \frac{4}{3}(G_i + G^*)}{K_i + \frac{4}{3}G_i + \pi\alpha\beta^*}\right], \tag{4}$$

$$\beta^* = G^*\frac{3K^* + G^*}{3K^* + 4G^*}, \tag{5}$$

where α is the mean aspect ratio of cracks (defined as $\alpha = w/c$), with c and w being the mean pore radius and aperture, respectively. These equations indicate that the effective elastic wave velocity under wet conditions can be predicted from its dry velocity if the relationships among elastic wave velocity, porosity, and aspect ratio for the Susaki cores are known.

Here, we use the relationships among elastic wave velocity, porosity, and aspect ratio for the Susaki cores that were obtained by Okuda et al. (2024), who measured the P- and S-wave velocities and porosity of discrete cylindrical samples taken from the core. Those authors found that the porosity of the core ranged from 1% to 4% and that the relationship between velocity and porosity generally fell between the trends for $\alpha = 0.01$ and $\alpha = 0.03$. We therefore assumed an average aspect ratio of 0.02 for modeling the wet velocities and porosity from the dry velocities that we measured. The porosity-free elastic moduli were taken to be $K_0 = 64$ GPa and $G_0 = 37$ GPa, which were estimated from the velocity–porosity relationship established for the Susaki cores (Okuda et al., 2024). The bulk modulus for the inclusion phase was set as 0 GPa for dry air and 2.2 GPa for water, whereas the shear modulus was 0 GPa for both conditions.

Effective medium models postulate non-isobaric conditions for pore fluid within any unit volume (i.e., representative elementary volume: REV) and are applicable to the high-frequency regime without equilibration of pore pressure (i.e., pore pressure differs from crack to crack) during loading. Here, the logging measurements were performed at a frequency of ~15 kHz, which can lie within the validity range of effective medium models (Fortin and Guéguen, 2021).

4 Results and discussion

4.1 Ultrasonic velocity profiles

Ultrasonic P-wave velocity profiles for each analyzed depth interval of the studies core are shown in Fig. 4a, c, and e. The velocity ranges broadly from 4 to 6 km/s, with a median of 5.44 km/s for all three layers. The sandstone layer has slightly higher velocity (median of 5.55 km/s) than the mudstone layers (median of 5.38 km/s). These results are consistent with laboratory results using discrete cylindrical samples taken from the Susaki cores (Okuda et al., 2024), are similar to high-velocity zones observed at the Nankai Trough (Kamei et al., 2013; Shiraishi et al., 2019), and are higher than those measured on other core samples from the Nankai subduction zone and the Shimanto accretionary complex (Hamahashi et al., 2013; Tsuji et al., 2006).

Fig. 4b, d, and f shows microscale porosity profiles estimated via the DEM model, assuming a mean crack aspect ratio of 0.02. The porosity ranges from 0.5% to 4%, with a median of 1.3%. The sandstone layer has slightly lower porosity (median of 1.1%) than the mudstone layers (median of 1.4%). Given the ultrasonic wavelength used here of 4–6 mm, these porosity variations indicate a heterogeneous distribution of millimeter to submillimeter scale defects. Microstructural observations of these core samples indicated that pressure solution processes, possibly driven by fluid migration, can have lowered the microcrack density and that variations in microscopic porosity are due mainly to variation in pore space along clay minerals, such as illite and chlorite (Okuda et al., 2024). Mineralogical analyses have also indicated that the mudstone samples have high clay mineral contents compared with the sandstones (Okuda et al., 2024), which is consistent with the relatively high porosity of the mudstone layers measured in this study. These observations suggest that the spatial variations in microscopic porosity can be attributed partly to clay mineral contents. Nevertheless, there are localized high-porosity zones, particularly in the sandstone layer (Fig. 4d), which may be attributable to localized areas of intense brittle damage.

To compare the ultrasonic velocity profiles measured under dry conditions with sonic logging velocity measured under water-saturated conditions, we modeled ultrasonic velocity under wet conditions from the dry velocity and porosity via DEM. The modeled velocities are higher than the dry velocities, ranging from 5.0 to 6.1 km/s (Fig. 5). Compared with the sonic logging velocities, these velocities are also higher by 0.1–2.1 km/s. This means that the observed sonic velocities cannot be explained by water-saturated microscopic

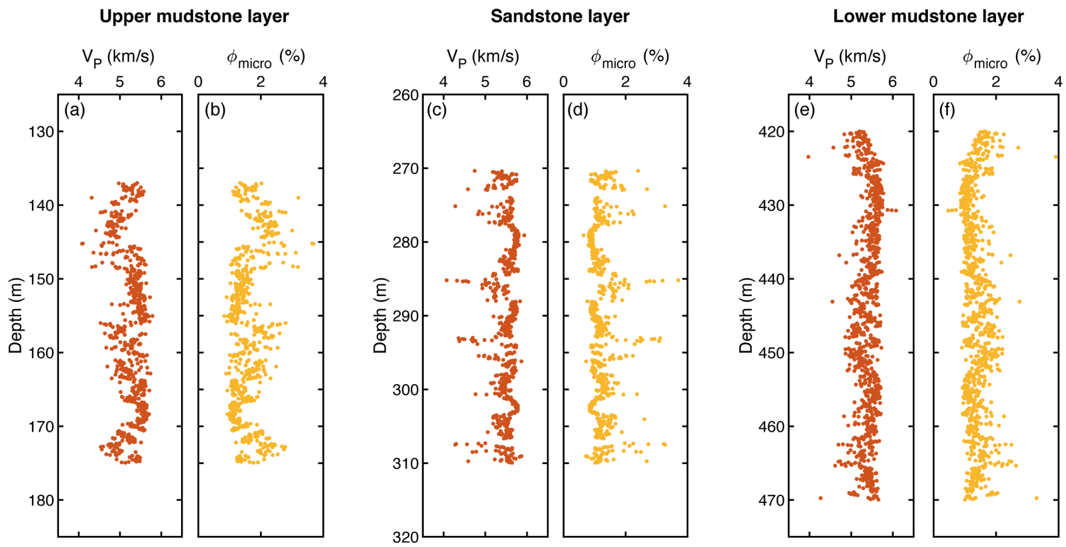

Fig. 4 Depth variations in ultrasonic P-wave velocity (a, c, and e) and microscale porosity estimated from the DEM model (b, d, and f) for each analyzed depth interval of the studies core.

porosity alone. Given that natural geological systems contain defects of different scales, the decrease in P-wave velocity of the Susaki core from ultrasonic to sonic scales implies the additional contribution of relatively large-scale porosities that are invisible via ultrasonic velocities.

4.2 Estimation of mesoscale porosity

To account for the discrepancies between the sonic and ultrasonic velocities, we introduced an effective medium model that includes mesoscale porosity in addition to microscale porosity, on the basis of DEM theory (Fig. 6). As described in the previous section, the effective elastic properties estimated via ultrasonic velocity can be expressed as a matrix phase containing (randomly oriented) penny-shaped cracks of a given mean aspect ratio (Eqs. 1, 2, 3, 4, 5). At the sonic wavelength scale (mesoscale), such an effective medium including microscopic porosity should be regarded as a matrix phase, and the effective elastic properties can be expressed by introducing a second family of mesoscale inclusions that are larger than the ultrasonic wavelength but smaller than the sonic wavelength (Fig. 6) (Bailly et al., 2019). Consequently, the effective elastic properties estimated via sonic velocity (K^{**} and G^{**}) can be expressed as follows:

$$(1-\phi_{\mathrm{meso}})\frac{d}{d\phi_{\mathrm{meso}}}[K^{**}(\phi_{\mathrm{meso}})] = (K_i - K^{**}(\phi_{\mathrm{meso}}))\,P^{**}(\phi_{\mathrm{meso}}), \tag{6}$$

$$(1-\phi_{\mathrm{meso}})\frac{d}{d\phi_{\mathrm{meso}}}[G^{**}(\phi_{\mathrm{meso}})] = (G_i - G^{**}(\phi_{\mathrm{meso}}))\,Q^{**}(\phi_{\mathrm{meso}}), \tag{7}$$

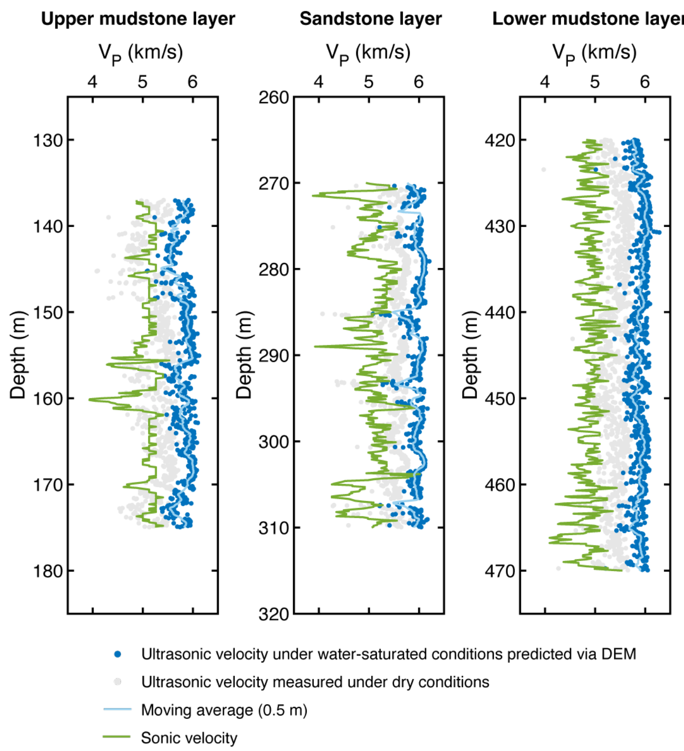

Fig. 5 Comparison of modeled P-wave velocity under water-saturated conditions (blue dots) with that predicted from dry velocity (gray dots) via DEM, with sonic logging velocities (green lines) for each analyzed depth interval of the studied core.

with the initial conditions $K^{**}(0) = K^*(\phi_{\text{micro}})$ and $G^{**}(0) = G^*(\phi_{\text{micro}})$, where ϕ_{micro} and ϕ_{meso} are the microscale and mesoscale porosities, respectively, and the total porosity is $\phi_{\text{total}} = \phi_{\text{micro}} + \phi_{\text{meso}}$. Here, we used P^{**} and Q^{**} for penny-shaped cracks assuming the mean aspect ratio of the mesoscale cracks to be 0.002. This value is based on a typical value for vein minerals that are traces of mesoscale fractures (van Everdingen, 1995). Using this model and the microscale porosity determined in the previous section, we performed an inversion of the observed sonic velocity and estimated mesoscale porosity. The microscale porosity used at each depth was a moving average of 0.5 m based on the sonic wavelength (Fig. 5).

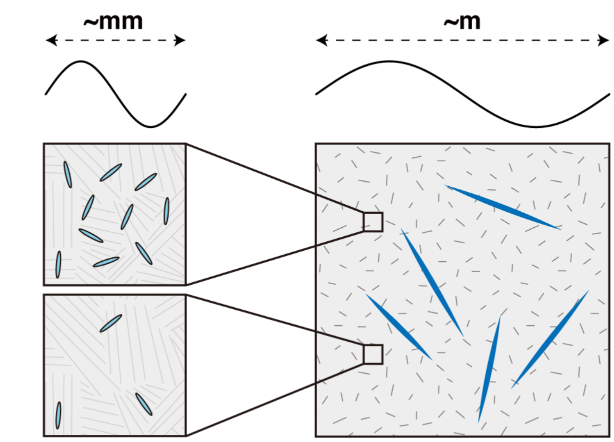

Fig. 6 Schematic illustrations showing modeling of effective elastic properties at the micro- and mesoscales by adding water-saturated microcracks and mesoscale fractures observed by different wavelengths (frequencies).

Fig. 7 shows the mesoscale porosity determined by the inversion of the sonic logging velocities, assuming a mean aspect ratio of mesoscale cracks of 0.002. The addition of mesoscale porosity of 0.1%–1.0% well explains the observed discrepancies between the ultrasonic and sonic velocities (Fig. S1). In contrast to the microscale porosity, the mesoscale porosity shows no clear difference between the sandstone layer (median of 0.5%) and the mudstone layers (median of 0.6%), implying that mesoscale fractures can develop regardless of lithology. According to the DEM model, mesoscale porosity with a low mean aspect ratio can readily decrease the elastic wave velocity compared with microscale porosity with a relatively high mean aspect ratio (Fig. 9a).

As described in the previous section, the DEM model is considered valid primarily for a relatively high-frequency regime ($\leq$kHz) where non-isobaric pore pressure conditions within the homogeneous unit volume (REV) can be assumed (e.g., Mavko et al., 2020). Thus, care should be taken when modeling the effect of porosity at seismic frequencies ($\ll$kHz). However, our dense data indicate that the spatial distributions of ultrasonic-scale (4–6 mm) and sonic-scale (0.3–0.4 m) porosities are not homogeneous at scales larger than their wavelengths, implying that a larger REV of porosity at each scale can be valid for the seismic frequencies in the order of a Hz (~km). This could prolong the time for the pore pressure equilibration within a given REV and extend the applicability of the effective medium model to even lower frequencies (Akamatsu et al., 2024).

Our model also assumes an isotropic orientation of fractures. Nevertheless, actual mesoscale fractures may exhibit anisotropy if they were formed under a deviatoric stress field. Although it is difficult to constrain the influence of anisotropy on the sonic velocity from our dataset alone, the presence of mesoscale fractures remains necessary even if the effect of anisotropy is ignored.

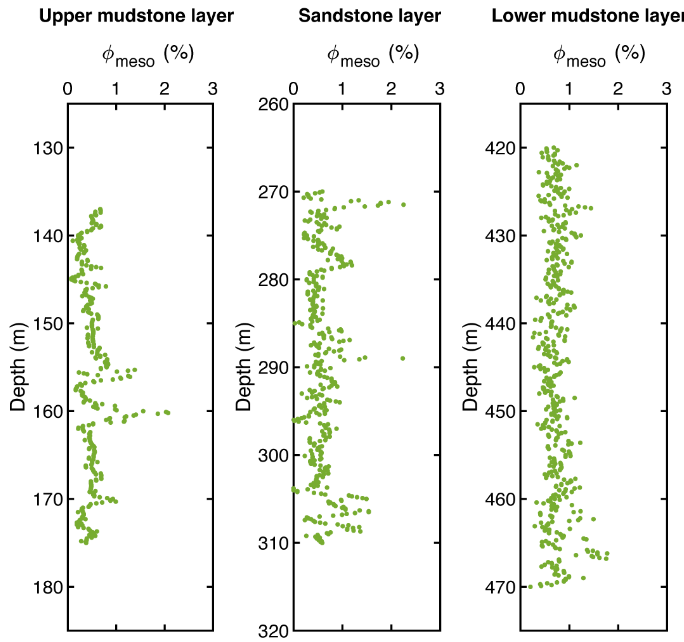

Fig. 7 Mesoscale porosity estimated for each analyzed depth interval of the studied core.

4.3 Role of mesoscale fractures in subduction zones

Numerous seismological surveys have been conducted in subduction zones to explore the relationship between seismic activity and geophysical structure. In the Nankai Trough, seismic velocity structure has been acquired by seismic reflection surveys and waveform inversion techniques, and low- and high-velocity anomalies have been identified in the hanging wall side of the plate boundary fault (Kamei et al., 2013; Shiraishi et al., 2019). Given the in situ lithostatic pressure, the identified low-velocity anomalies have been interpreted as an indicator of extremely high pore-fluid pressure close to the lithostatic pressure (i.e., low effective pressure) that can maintain open pore spaces (Kitajima and Saffer, 2012; Tsuji et al., 2014). This interpretation of velocity anomalies has been attributed to microscale pore space only because it is based on the velocity–porosity relationship for subduction-zone rocks established at ultrasonic frequency, i.e., microscale pore space (Hoffman and Tobin, 2004; Tsuji et al., 2006). However, our results demonstrate that the P-wave velocity of subduction-zone rocks can readily decrease down to 5 km/s or even lower when a part of the total porosity is accommodated by the mesoscale fractures (Fig. 9a). As the Susaki core without mesoscale fractures (i.e., measurements at the ultrasonic frequency) shows high velocities similar to those of high-velocity zones along the Nankai Trough, the variations in the seismic velocity observed in the Nankai Trough may reflect the distribution of mesoscale fractures with high pore pressure.

It is to be noted that our estimates of mesoscale porosities for the Susaki cores could be formed during their exhumation processes. Thus, the mesoscale fractures estimated from the sonic logging at the Susaki boreholes are not the ones which are in deep subduction zones. In fact, fluid-saturated fractures that were present at subduction plate interfaces can now be observed as veins (Muñoz-Montecinos and Behr, 2023; Otsubo et al., 2020; Ujiie et al., 2018). The Susaki cores commonly contain quartz veins with apertures of several tens to hundreds of microns (Fig. 8). Such veins are possibly remnants of mesoscale fractures under high pore fluid pressure in the deep subduction zone before exhumation and likely affected seismic velocities in the subduction zones.

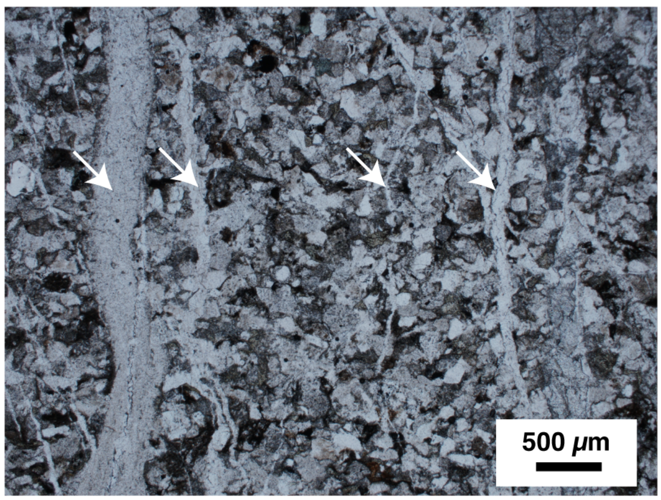

Fig. 8 Representative photomicrographs (plane-polarized light) of sandstone from the Susaki core showing quartz veins (white arrows) with apertures of several tens to hundreds of microns.

Fluid migration through pore spaces may trigger characteristic seismic activity in subduction zones (e.g., Tonegawa et al., 2022). The mesoscale fractures can act as effective fluid pathways and facilitate rapid fluid drainage in the deep subduction zone, since permeability of rock is also scale-dependent (Heap and Kennedy, 2016). The effective permeability of rock containing randomly oriented penny-shaped cracks k is given as follows:

$$k = \frac{2}{15} f \phi w^2, \tag{8}$$

where f is the connectivity of pore space ($0 \leq f \leq 1$), ϕ is the porosity, and w is the mean aperture of cracks (Guéguen and Palciauskas, 1994). This equation predicts the permeability to be strongly dependent on crack aperture. For a rock mass containing micro- and mesoscale porosities, the effective permeability can be expressed as follows:

$$k = k_{\mathrm{micro}} + k_{\mathrm{meso}} = \frac{2}{15}(f_{\mathrm{micro}}\phi_{\mathrm{micro}}w^2_{\mathrm{micro}} + f_{\mathrm{meso}}\phi_{\mathrm{meso}}w^2_{\mathrm{meso}}), \tag{9}$$

where the subscripts denote each scale. Here, we incorporated this model into our upscaled DEM model and estimated the relationship between V_{P} and k for subduction zones, which accounts for the scaling effect. First, we calculated V_{P} and k for microscale porosity until V_{P} reaches the median of ultrasonic velocity of the Susaki core with a mean aspect ratio of 0.02. w_{micro} was set as 1 µm, based on microstructural observations (Okuda et al., 2024). We then added mesoscale porosity into the matrix phase with the microscale V_{P} and k until V_{P} reaches the median of sonic velocity of the Susaki area with a mean aspect ratio of 0.002. w_{meso} was set as 100 µm, based on the sonic wavelength and the assumed aspect ratio. Since the connectivity of pore space is not measurable from our data, we assumed $f = 1$ for each scale, and the estimated permeability should therefore be considered as the maximum value.

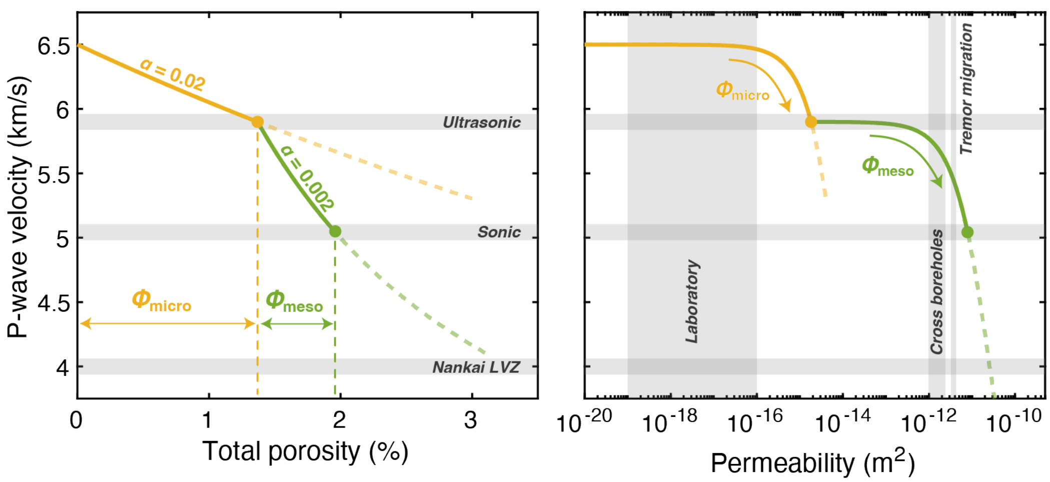

Fig. 9 (a) P-wave velocity as a function of total porosity modeled for the median values of ultrasonic and sonic velocities obtained in this study (gray lines). Data from a low-velocity zone (LVZ) in the Nankai Trough (Shiraishi et al., 2019) is also presented. (b) Relationship between P-wave velocity and permeability modeled by incorporating micro- and mesoscale porosities. The vertical gray shadings represent values obtained from laboratory measurements using drill core samples from the Nankai Trough (Song and Underwood, 2017; Takahashi et al., 2013; Valdez et al., 2015), a cross-hole experiment in the Nankai Trough (Kinoshita and Saffer, 2018), and constraints based on tremor migration patterns observed in the Nankai Trough (Hendriyana and Tsuji, 2021).

Fig. 9b shows the relationship between V_{P} and k modeled using the upscaled DEM model. The permeability initially increases by several orders of magnitude with decreasing velocity. As ϕ_{micro} increases, k increases up to 10^{-15} to 10^{-14} m^2 with a slight decrease in V_{P}, but the the rate of increase in permeability becomes more gradual once ϕ_{micro} no longer changes by orders of magnitude. Although these permeability values are 1–2 orders of magnitude higher than those typically measured for hand-sized sedimentary rocks in the laboratory (Song and Underwood, 2017; Takahashi et al., 2013; Valdez et al., 2015), this is likely resulted from a fixed crack aperture and assumption of perfectly connected pore spaces. When the effects of mesoscale porosity are included, k further increases by several orders of magnitude as V_P continues to decrease. Eventually, k increases to the order of 10^{-12} to 10^{-11} m^2 as V_P decreases to those of the sonic velocity in the Susaki area and a low-velocity zone in the Nankai Trough (Shiraishi et al., 2019). These permeability values cover the range of permeability determined at a scale of ~100 m by a cross-hole experiment in the Nankai Trough (Kinoshita and Saffer, 2018). Such high permeability values are also required to explain tremor migration patterns observed in the Nankai subduction zone, which may represent fracture permeability that was enhanced during slow slip events (Hendriyana and Tsuji, 2021). Our results suggest that mesoscale fractures constitute highly permeable and low-velocity regions where characteristic seismic activity occurs in subduction zones. In fact, temporal changes in seismic velocity structure observed in the Nankai subduction zone have been shown to be associated with fluid migration before slow earthquakes (Tonegawa et al., 2022).

5 Conclusions

To explore the scale dependence of seismic velocity in subduction zones, we compared ultrasonic and sonic velocities of core samples from the Susaki area in the Cretaceous Shimanto accretionary complex. The comparison revealed a decrease in P-wave velocity from ~6 to 5 km/s with increasing scale, which we explain by accounting for mesoscale porosity. This finding indicates that low-velocity anomalies observed along the Nankai Trough may be associated with the presence of mesoscale fractures with high pore pressure. Mesoscale fractures can also lead to high permeability in subduction zones of up to 10^{-12} to 10^{-11} m^2 and hence effective fluid drainage. Seismic activity related to transient fluid migration around low-velocity zones could therefore be associated with the occurrence of the mesoscale fractures.

Declaration of competing interest

The authors declare no conflicts of interest.

Acknowledgements

We thank Satoshi Itaba (GSJ) for allowing the use of core samples and Tsutomu Kiguchi (GSJ) for providing detailed information on borehole logging measurements. We are grateful to Takahiro Suzuki (MWJ), Osamu Tadai (MWJ), and Rina Fukuchi (Naruto Education Univ.) for supporting the laboratory measurements. This study was supported by JSPS KAKENHI grants JP24H01039 (Grant-in-Aid for Transformative Research Areas (A) “Science of Slow-to-Fast Earthquakes”) for Y. Akamatsu, JP23K19081 (Grant-in-Aid for Research Activity Start-up) and JP24H01036 (Grant-in-Aid for Transformative Research Areas (A) “Science of Slow-to-Fast Earthquakes”) for H. Okuda, and JP22K14112 (Grant-in-Aid for Early-Career Scientists) for M. Sawai.

Data availability

All the laboratory data and borehole logging data used in this study are provided in the Supplementary Materials.

References

Akamatsu, Y., Kuwatani, T., Katayama, I., 2024. Spatial heterogeneity of pore structure in the crustal section of the samail ophiolite: Implications for high VP/VS anomalies in subducting oceanic crust. Geophysical research letters 51, e2023GL106943. https://doi.org/10.1029/2023GL106943

Akamatsu, Y., Nagase, K., Abe, N., Okazaki, K., Hatakeyama, K., Katayama, I., 2023. Cross-property relationship between electrical resistivity and elastic wave velocity of crustal rocks from the oman drilling project hole GT3A: Implications for in situ geophysical properties of oceanic crust. Journal of Geophysical Research, [Solid Earth] 128. https://doi.org/10.1029/2022jb026130

Audet, P., Schwartz, S.Y., 2013. Hydrologic control of forearc strength and seismicity in the costa rican subduction zone. Nature geoscience 6, 852–855. https://doi.org/10.1038/ngeo1927

Bailly, C., Fortin, J., Adelinet, M., Hamon, Y., 2019. Upscaling of elastic properties in carbonates: A modeling approach based on a multiscale geophysical data set. Journal of Geophysical Research, [Solid Earth] 124, 13021–13038. https://doi.org/10.1029/2019jb018391

Berryman, J.G., Pride, S.R., Wang, H.F., 2002. A differential scheme for elastic properties of rocks with dry or saturated cracks. Geophysical Journal International 151, 597–611. https://doi.org/10.1046/j.1365-246X.2002.01801.x

Eberhart-Phillips, D., Bannister, S., Reyners, M., 2017. Deciphering the 3-D distribution of fluid along the shallow hikurangi subduction zone using P- and S-wave attenuation. Geophysical Journal International 211, 1032–1045. https://doi.org/10.1093/gji/ggx348

Fortin, J., Guéguen, Y., 2021. Porous and cracked rocks elasticity: Macroscopic poroelasticity and effective media theory. Mathematics and mechanics of solids: MMS 26, 1158–1172. https://doi.org/10.1177/10812865211022034

Guéguen, Y., Palciauskas, V., 1994. Introduction to the physics of rocks. Princeton University Press.

Hamahashi, M., Saito, S., Kimura, G., Yamaguchi, A., Fukuchi, R., Kameda, J., Hamada, Y., Kitamura, Y., Fujimoto, K., Hashimoto, Y., Hina, S., Eida, M., 2013. Contrasts in physical properties between the hanging wall and footwall of an exhumed seismogenic megasplay fault in a subduction zone-an example from the nobeoka thrust drilling project. Geochemistry, Geophysics, Geosystems 14, 5354–5370. https://doi.org/10.1002/2013gc004818

Hashimoto, Y., Eida, M., Kirikawa, T., Iida, R., Takagi, M., Furuya, N., Nikaizo, A., Kikuchi, T., Yoshimitsu, T., 2012. Large amount of fluid migration around shallow seismogenic depth preserved in tectonic mélange: Yokonami mélange, the cretaceous shimanto belt, kochi, southwest japan. Island Arc 21, 53–64. https://doi.org/10.1111/j.1440-1738.2011.00806.x

Heap, M.J., Kennedy, B.M., 2016. Exploring the scale-dependent permeability of fractured andesite. Earth and planetary science letters 447, 139–150. https://doi.org/10.1016/j.epsl.2016.05.004

Hendriyana, A., Tsuji, T., 2021. Influence of structure and pore pressure of plate interface on tectonic tremor in the nankai subduction zone, japan. Earth and planetary science letters 558, 116742. https://doi.org/10.1016/j.epsl.2021.116742
Hoffman, N.W., Tobin, H.J., 2004. An empirical relationship between velocity and porosity for underthrust sediments in the nankai trough accretionary prism. Proc. Ocean Drill. Program Sci. Results, 190 196, 1–23.
Ide, S., 2010. Striations, duration, migration and tidal response in deep tremor. Nature 466, 356–359. https://doi.org/10.1038/nature09251
Itaba, S., Umeda, Y., Koizumi, N., Watanabe, H., Nakayama, N., Sakai, S., 2014. Geological data of the GSJ boring core at the susaki-otani observation station (No. 595). Geol. Surv. Japan, AIST.
Kamei, R., Pratt, R.G., Tsuji, T., 2013. On acoustic waveform tomography of wide-angle OBS data—strategies for pre-conditioning and inversion. Geophysical Journal International 194, 1250–1280. https://doi.org/10.1093/gji/ggt165
Kinoshita, C., Saffer, D.M., 2018. In situ permeability and scale dependence of an active accretionary prism determined from cross-borehole experiments. Geophysical research letters 45, 6935–6943. https://doi.org/10.1029/2018gl078304
Kitajima, H., Saffer, D.M., 2012. Elevated pore pressure and anomalously low stress in regions of low frequency earthquakes along the nankai trough subduction megathrust. Geophysical research letters. https://doi.org/10.1029/2012GL053793
Kitamura, M., Hirose, T., Lei, X., 2021. Mechanical weakness of the nankai accretionary prism: Insights from V p measurements of drill cuttings. Geochemistry, Geophysics, Geosystems 22. https://doi.org/10.1029/2020gc009536
Matonti, C., Guglielmi, Y., Viseur, S., Bruna, P.O., Borgomano, J., Dahl, C., Marié, L., 2015. Heterogeneities and diagenetic control on the spatial distribution of carbonate rocks acoustic properties at the outcrop scale. Tectonophysics 638, 94–111. https://doi.org/10.1016/j.tecto.2014.10.020
Mavko, G., Mukerji, T., Dvorkin, J., 2020. The rock physics handbook. Cambridge University Press.
Muñoz-Montecinos, J., Behr, W.M., 2023. Transient permeability of a deep-seated subduction interface shear zone. Geophysical research letters 50. https://doi.org/10.1029/2023gl104244
Okuda, H., Akamatsu, Y., Kitamura, M., Sawai, M., 2024. Elastic properties of hanging wall rock at the seismogenic zone and critical nucleation length for megathrust earthquakes. ESS Open Archive. https://doi.org/10.22541/essoar.171838469.98902412/v1
Otsubo, M., Hardebeck, J.L., Miyakawa, A., Yamaguchi, A., Kimura, G., 2020. Localized fluid discharge by tensile cracking during the post-seismic period in subduction zones. Scientific reports 10, 12281. https://doi.org/10.1038/s41598-020-68418-z
Raimbourg, H., Hamano, Y., Saito, S., others, 2011. Acoustic and mechanical properties of nankai accretionary prism core samples. Geochemistry: Exploration, Environment, Analysis. https://doi.org/10.1029/2010GC003169
Saffer, D., 2003. Pore pressure development and progressive dewatering in underthrust sediments at the costa rican subduction margin: Comparison with northern barbados and nankai. Journal of geophysical research 108, 2261. https://doi.org/10.1029/2002JB001787
Saffer, D.M., Tobin, H.J., 2011. Hydrogeology and mechanics of subduction zone forearcs: Fluid flow and pore pressure. Annual review of earth and planetary sciences 39, 157–186. https://doi.org/10.1146/annurev-earth-040610-133408

Sakaguchi, A., 1999. Thermal maturity in the shimanto accretionary prism, southwest japan, with the thermal change of the subducting slab: Fluid inclusion and vitrinite reflectance study. Earth and planetary science letters 173, 61–74. https://doi.org/10.1016/S0012-821X(99)00219-8

Sarout, J., Ferjani, M., Guéguen, Y., 2009. A semi-automatic processing technique for elastic-wave laboratory data. Ultrasonics 49, 452–458. https://doi.org/10.1016/j.ultras.2008.12.001

Shiraishi, K., Moore, G.F., Yamada, Y., Kinoshita, M., Sanada, Y., Kimura, G., 2019. Seismogenic zone structures revealed by improved 3-D seismic images in the nankai trough off kumano. Geochemistry, Geophysics, Geosystems. https://doi.org/10.1029/2018gc008173

Song, C., Underwood, M.B., 2017. Data report: Permeability and microfabric of core samples from IODP expedition 348, hole C0002P, nankai trough accretionary prism, in: Proceedings of the IODP, Proceedings of the Integrated Ocean Drilling Program . Integrated Ocean Drilling Program. Integrated Ocean Drilling Program. https://doi.org/10.2204/iodp.proc.348.201.2017

Taira, A., 1988. The shimanto belt in shikoku, japan-evolution of cretaceous to miocene accretionary prism. Shimanto Belt, Modern Geology 12, 5–46.

Takahashi, M., Azuma, S., Uehara, S.-I., Kanagawa, K., Inoue, A., 2013. Contrasting hydrological and mechanical properties of clayey and silty muds cored from the shallow nankai trough accretionary prism. Tectonophysics, Proceedings of the integrated ocean drilling program 314/315/316Mechanical behavior of crustal RocksProceedings of the integrated ocean drilling program 314/315/316Fault mechanics and transport properties of RocksProceedings of the integrated ocean drilling program 314/315/316The seismogenic zone of subduction thrust FaultsAmerican geophysical union 2008 fall meeting, T31A-1980Proceedings of the integrated ocean drilling program 314/315/316Physical properties of rocks: Fundamentals and principles of PetrophysicsProceedings of the integrated ocean drilling program 314/315/316The seismogenic zone of subduction thrust faults 600, 63–74. https://doi.org/10.1016/j.tecto.2013.01.008

Tonegawa, T., Takemura, S., Yabe, S., Yomogida, K., 2022. Fluid migration before and during slow earthquakes in the shallow nankai subduction zone. Journal of Geophysical Research, [Solid Earth] 127. https://doi.org/10.1029/2021jb023583

Tsuji, T., Kamei, R., Pratt, R.G., 2014. Pore pressure distribution of a mega-splay fault system in the nankai trough subduction zone: Insight into up-dip extent of the seismogenic zone. Earth and planetary science letters 396, 165–178. https://doi.org/10.1016/j.epsl.2014.04.011

Tsuji, T., Kimura, G., Okamoto, S., Kono, F., Mochinaga, H., Saeki, T., Tokuyama, H., 2006. Modern and ancient seismogenic out-of-sequence thrusts in the nankai accretionary prism: Comparison of laboratory-derived physical properties and seismic reflection data. Geophysical research letters 33. https://doi.org/10.1029/2006GL027025

Ujiie, K., Saishu, H., Fagereng, Å., Nishiyama, N., Otsubo, M., Masuyama, H., Kagi, H., 2018. An explanation of episodic tremor and slow slip constrained by crack-seal veins and viscous shear in subduction mélange. Geophysical research letters 45, 5371–5379. https://doi.org/10.1029/2018gl078374

Valdez, R.D., II, Lauer, R.M., Ikari, M.J., Kitajima, H., Saffer, D.M., 2015. Data report: Permeability and consolidation behavior of sediments from the northern japan trench subduction zone, IODP site C0019, in: Proceedings of the IODP, Proceedings of the Integrated Ocean Drilling Program . Integrated Ocean Drilling Program. Integrated

Ocean Drilling Program. https://doi.org/10.2204/iodp.proc.343343t.201.2015
van Everdingen, 1995. Fracture characteristics of the sheeted dike complex, troodos ophiolite, cyprus: Implications for permeability of oceanic crust. Journal of geophysical research 100, 19957–19972. https://doi.org/10.1029/95JB01575